Available online at www.sciencedirect.com

SciVerse ScienceDirect

journal homepage: www.elsevier.com/locate/he

Effect of alloying elements on hydrogen environment embrittlement of AISI type 304 austenitic stainless steel

M. Martin [a,*], S. Weber [a,b], W. Theisen [a], T. Michler [c], J. Naumann [d]

[a] Ruhr-Universität Bochum, Institut für Werkstoffe, Lehrstuhl Werkstofftechnik, D-44780 Bochum, Germany
[b] Helmholtz-Zentrum Berlin für Materialien und Energie GmbH, D-14109 Berlin, Germany
[c] Adam Opel AG, Ruesselsheim, Germany
[d] BMW AG, Munich, Germany

ARTICLE INFO

Article history:
Received 11 May 2011
Received in revised form
31 August 2011
Accepted 2 September 2011
Available online 29 September 2011

Keywords:
Austenitic stainless steel
Hydrogen environment embrittlement
Austenite stability
Strain induced martensite
Calphad

ABSTRACT

The chemical composition of an AISI type 304 austenitic stainless was systematically modified in order to evaluate the influence of the elements Mo, Ni, Si, S, Cr and Mn on the material's susceptibility to hydrogen environment embrittlement (HEE). Mechanical properties were evaluated by tensile testing at room temperature in air at ambient pressure and in a 40 MPa hydrogen gas atmosphere. For every chemical composition, the corresponding austenite stability was evaluated by magnetic response measurements and thermodynamic calculations based on the Calphad method. Tensile test results show that yield and tensile strength are negligibly affected by the presence of hydrogen, whereas measurements of elongation to rupture and reduction of area indicate an increasing ductility loss with decreasing austenite stability. Concerning modifications of alloy composition, an increase in Si, Mn and Cr content showed a significant improvement of material's ductility compared to other alloying elements.

1. Introduction

The way to renewable energy sources is highly dependent on the availability of new materials which must fulfil certain performance depending on the specific application, safety requirements, and last but not least, cost efficiency. A global implementation of renewable energies will demand, accordingly, affordable and globally available materials. That is the reason why many efforts are carried out to incorporate steels into new technologies. In the particular case of hydrogen applications, most metallic materials suffer a deterioration of mechanical properties by getting in contact with any hydrogen source [1]; usually referred as hydrogen embrittlement (HE). In this context, austenitic stainless steels constitute a very attractive alternative. For instance, high alloyed austenitic stainless steels like AISI type 316L and 310 are characterized by a high resistance against HE at room temperature [2,3]; however, their use in a massive scale is impracticable as a consequence of the materials costs. On the other hand, the alternative of less alloyed austenitic steel, like AISI type 304, results in a less expensive but metastable structure which leads to a non-sufficient ductility response [4].

For the design of any component involved in containing or conducting hydrogen, it is essential to know how the material's mechanical properties are affected by the mentioned environment. In this scope, tensile testing in external hydrogen is frequently employed as it also allows to evaluate the effect of gas pressure, gas purity and temperature on the

* Corresponding author.
E-mail address: martin@wtech.rub.de (M. Martin).
0360-3199/$ – see front matter
doi:10.1016/j.ijhydene.2011.09.013

material's mechanical response. Nevertheless, comparison of mechanical properties obtained via this method have to be done carefully, as they are known to be strongly dependant on other parameters like strain rate [5], and particularly, on the internal hydrogen content, i.e., whether the material has been or has not been precharged.

Finally, the aim of this work is to characterize the influence of the main alloying elements of AISI 304 steel on HEE in order to contribute to an alloy optimization process, capable of combining acceptable performance together with relatively low cost. In this context, mechanical properties are related to austenite stability which was both experimentally and thermodynamically evaluated, with a very good agreement between the two methodologies. Results are compared to a highly resistant 17Cr-12.2Ni-2.4Mo steel as a reference.

2. Experimental

2.1. Sample production

Tensile specimens were produced out of two different sources, laboratory scale cast material and commercially available material in the compositional range of AISI type 304 steel. The first alternative was used in order to modify Cr and Mo content (not available in commercial grades); whereas the second one provided the compositions varying Si, Mn, S and Ni content.

Laboratory heats consisted in the remelting of a base material, designated as 11 (AISI type 304) in this work, with the corresponding additions to increase Cr and Mo content. Materials designated as 11-R (remelted), 11-Cr and 11-Mo were produced in a vacuum induction furnace under an 80 kPa argon gas pressure. As cast ingots with a weight of 3 kg and a diameter of 50 mm were pre-machined and hot worked in several passes to a final diameter of 16 mm, followed by water quenching. Commercially available material was provided by Deutsche Edelstahlwerke (DEW, Germany). It was continuously casted in a 265 mm square cross section and subsequently hot rolled to a bar shape with a final diameter of 30 mm. The absence of macroscopic segregation was confirmed by measuring chemical composition on the radial direction of 16 mm and 30 mm diameter materials by means of optical spark emission spectrometry. In both cases, the small cross section and high cooling rate lead to a very homogenous composition. Additionally, all tensile specimens were produced from the center of the as forged bars to minimize differences in chemical composition.

For every chemical composition four cylindric tensile specimens with a gauge length of 30 mm and a diameter of 5 mm were produced by wet turning, with a mean surface roughness of $R_a < 0.4$ μm. In order to minimize surface related influence on hydrogen embrittlement [6], tensile specimens were solution annealed for 30 min at 1050 °C in an industrial vacuum furnace equipped with graphite heaters, and argon gas quenched at a pressure of 200 kPa. Cooling rates from solution annealing temperature were high enough to ensure a fully austenitic microstructure free of precipitates. After solution annealing, the resulting grain size for both production routes was 45 μm ± 5 μm (ASTM grain size number $G = 6.0$). Table 1 presents the chemical compositions of the studied materials measured on tensile specimens by optical spark emission spectrometry. In this regard, alloy 11 has been used for evaluating three different states: high silicon, low sulphur and high manganese condition.

2.2. Tensile tests

Tensile tests in air and in pure hydrogen gas (≥99.9999% H_2) were carried out for all compositions at a temperature of 25° ± 3°. Ambient pressure was used for the air tested specimens while 40 MPa were applied for the tests in hydrogen atmosphere. For hydrogen testing, the vessel was purged three times with pure nitrogen at 1 MPa. Subsequently, eight consecutive purges with pure hydrogen at 1 MPa took place before filling to test pressure. This procedure ensures safety and gas purity. In both air and hydrogen testing, an initial strain rate of $5.5 \cdot 10^{-5} s^{-1}$ was used according to ASTM G129 standard. At room temperature this strain rate is slow enough to allow hydrogen atoms to migrate with moving dislocations and influence the deformation mechanism [7]. For the case of hydrogen testing, load was measured using an external load cell with allowance for the frictional force, which was constant over the full displacement at constant displacement rate. Clip gauge/extensometer measurements were used in

Table 1 – Chemical composition of the investigated austenitic stainless steel; values in mass-% with iron being the dependent substitutional element. Alloy 11 serves as reference for elements Si, S and Mn while alloy 11-R does it for Mo and Cr elements.

Element	Material	C	Si	Mn	P	S	Cr	Ni	Mo	N	Cu
Mo	11-Mo	0.018	0.701	1.909	0.029	0.031	17.78	8.63	0.983	0.0727	0.635
	11-R	0.018	0.691	1.958	0.029	0.03	17.7	8.66	0.296	0.0751	0.64
Ni	2	0.016	0.628	1.935	0.03	0.029	17.76	8.95	0.334	0.0615	0.523
	3	0.021	0.689	1.925	0.03	0.023	17.67	8.38	0.283	0.0627	0.608
Si	11	0.018	0.686	1.965	0.028	0.028	17.79	8.49	0.293	0.0696	0.624
	9	0.019	0.403	1.858	0.026	0.028	17.66	8.11	0.35	0.0982	0.33
S	1	0.043	0.61	1.78	0.026	0.255	17.7	8.48	0.312	0.0444	0.716
Cr	11-Cr	0.018	0.686	1.965	0.029	0.029	18.74	8.67	0.291	0.0712	0.635
Mn	8	0.014	0.569	1.042	0.025	0.016	17.89	8.23	0.201	0.0849	0.278
Ref.	12	0.012	0.826	1.433	0.028	0.021	17.13	12.24	2.465	0.0572	0.349
	CN0.96	0.321	0.25	19.31	0.022	0.002	17.39	0.31	0.056	0.626	0.043

air/hydrogen environments for determination of 0.2% proof stress. Measured properties were yield strength (Rp_{02}), ultimate tensile strength (R_m) and elongation to rupture (A). Additionally, values of reduction of area (Z) were obtained by measuring the specimen's diameter with a caliper at the necking circumference, as this parameter is known to be very sensitive to hydrogen embrittlement [3,8].

2.3. Austenite stability

2.3.1. Ferrite equivalent and M_{d30} temperature

Before and after tensile testing, a ferrite equivalent value was determined for every sample using a FeritScope® MP30 device (Helmut Fischer GmbH, Sindelfingen, Germany) which employs the magnetic induction method in the quantification of ferromagnetic phases. Accordingly, measurements before testing reveal remaining δ – ferrite phase content in the austenitic matrix, while subsequent readings are able to show the contribution of strain-induced martensite, as it is expected to form at the investigated compositional range. In order to avoid contributions from inhomogeneous plastic deformation after tensile testing, ferrite equivalent was determined by carrying out four measurements radially distributed at the midpoint of the uniformly elongated region. Additionally, M_{d30} temperature was calculated as a complimentary parameter for assessing the tendency of every alloy to undergo strain-induced transformation, according to Nohara's formula [9] given in Eq. (1).

$$M_{d30} = 551 - 462\cdot wt\%(C+N) - 9.2\cdot wt\%Si - 8.1\cdot wt\%Mn - 13.7\cdot wt\%Cr - 29\cdot wt\%Ni - 18.5\cdot wt\%Mo - 29\cdot wt\%Cu - 68\cdot wt\%Nb - 1.42\cdot(\text{grain size [ASTM]} - 8.0) \quad (1)$$

2.3.2. Thermodynamic calculations

Austenite stability was thermodynamically evaluated as the difference in Gibbs free energy between the austenite and ferrite phase for a fixed composition at 298.15 K, as shown in Eq. (2) [10]. Due to the same chemical composition is assumed for ferrite and austenite phase, Gibbs energy was calculated imposing a metastable state instead of a thermodynamic equilibrium. This approach was successfully applied by other authors for calculating stacking fault energies of austenitic steels by means of thermodynamic data [11,12]. A negative value for $\Delta G_{\gamma/\alpha}$ would indicate that the bcc phase is thermodynamically stable at room temperature, and consequently the fcc phase can decompose into a bcc one. Therefore, this energy difference may be interpreted as an approximation to the available driving force for martensitic transformation. Corresponding calculations were based on the Calphad method and performed with the software ThermoCalc® S together with the database TCFE6.2. In this regard, the full compositions (c.f. Table 1) were employed with the exception of the element phosphor. This element is not expected to influence thermodynamic calculation due to its constant and low concentration in all alloys. Furthermore, all thermodynamic calculations rely on the assumption of a fully homogeneous austenite with all alloying elements in solid solution. The influence of microsegregations was not considered in thermodynamic calculations for the sake of simplicity. This approach is consistent with the use of Md_{30} formula, as it can be found in numerous others works.

$$\Delta G_{\gamma/\alpha} = G_{bcc} - G_{fcc} \quad (2)$$

2.3.2.1. Brief overview of the CALPHAD method

The CALPHAD method (CALculation of PHAse Diagrams) refers to a thermodynamic approach for describing thermodynamic properties and phase diagrams of multicomponent and multiphase systems. The method is based on the assessment of the Gibbs energy as a function of composition, temperature and pressure. Different models are used for assessing Gibbs energy function depending on the nature of the considered phase. Those models are coupled with thermodynamic databases which contain experimental data for pure substances and multicomponent systems. Thereby, the assessment of Gibbs energy results from models and databases coupled in computational calculations. Moreover, many other important thermodynamic properties can be derived from the Gibbs energy, like enthalpy, entropy and chemical potential. In this manner, the method is able to predict thermodynamic equilibrium by minimization of Gibbs energy function and also to extrapolate thermodynamic functions outside of equilibrium, for instance to describe metastable states [13–15].

3. Results

3.1. Tensile tests

Whit the exception of alloy 12, all tested materials have shown ductility losses with different severity. While air testing resulted in typical cup-cone ruptures characterize by a microvoid coalescence, hydrogen testing resulted in brittle fractures with faceted surfaces showing a quasi-cleavage failure mode. Representative stress-stain curves and fractographic pictures for air and hydrogen testing are shown in Figs. 1 and 2 for alloy 8, respectively. Tensile properties measured in air and hydrogen gas atmosphere are listed in Table 2. Every value is the average of two results obtained in

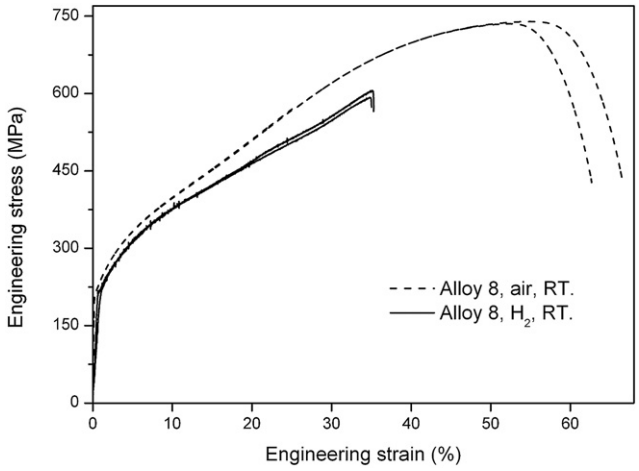

Fig. 1 – Engineering stress-strain curves of alloy 8 obtained in air (p = 0.1 Mpa) and hydrogen gas (p = 40 MPa) at 25 °C.

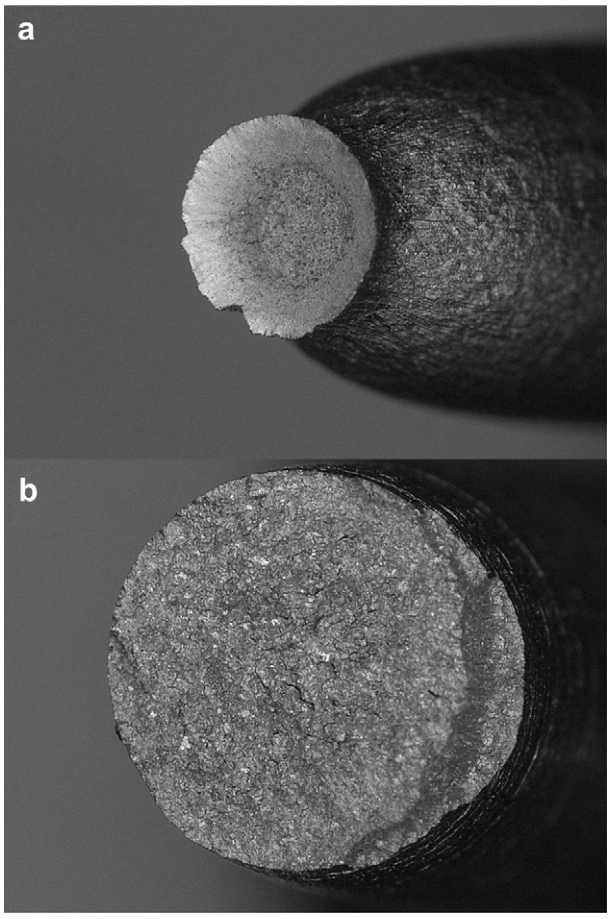

Fig. 2 – Fracture surface of alloy 8 after testing at 25 °C: a) air atmosphere, $p = 0.1$°Mpa; b) hydrogen gas, $p = 40$ MPa.

the same condition. As can be seen, two columns appear for every property, on the left hand side the values for hydrogen testing and on the right the air testing results. In order to ease comparison, mechanical properties are presented graphically in their relative form, i.e. as the ratio between hydrogen and air results, including corresponding scatter in Figs. 3 to 6. The first figure shows that relative yield strength (RRp_{02}) is almost unaffected by the present testing conditions, since all average values lie between 95 and 100%, being additionally overlapped by scatter bars. The same deviation occurs for Si, S and Mn elements due to experimental scatter by hydrogen testing of alloy 11; which was used as a reference for this three elements. Fig. 4 presents the relative tensile strength. Here, with the exception of alloy 8 ($Mn_{1.04}$), results are spread between the 90–100% band indicating a rather small influence of the hydrogen atmosphere on R_m. The situation changes considerably when the relative elongation to rupture is considered (c.f. Fig. 5). In this case, differences in average values start to be more significant and consequently, some trends can be identified. In particular, mean values for different Ni, Si and Mn contents are clearly separated indicating an increase of ductility response for higher contents of these elements. Relative reduction of area (RZ) results are presented in Fig. 6. Such values arise from an ex-situ measurement of the specimen's final diameter after testing. As can be seen, the embrittlement becomes rather noticeable. In particular, average values are clearly different, scatter becomes quite small and free of overlapping. The reference material, designated as 12, is the only one capable of reaching a RZ of 100%. For all others steels it is clear that an increase in alloying element content leads to a higher reduction of area, i.e. higher ductility. As already mentioned, it is important to note that results for alloy 11 are presented three times in each figure as it was employed as reference in testing the influence of the elements Si, S and Mn.

In order to evaluate how effective or efficient is the alloying process in every case, an impact factor was defined for all elements taking into account changes of chemical composition and average values for elongation to rupture and reduction of area (c.f. Table 3). Here, the second column ($Element_{ratio}$) represents the change of the element of interest, as the ratio between higher and lower content. In the same manner, third and fourth columns show the ratio in A and Z between the "high" and "low-alloyed" variant. Both columns are subsequently normalized to the $Element_{ratio}$ in the A_r Norm. and Z_r Norm., respectively. Finally, an impact factor is obtained as the product of the last two columns. According to this, Cr, Ni, Mn and Si, in that order, contribute strongly to ductility improvement in the investigated composition range. While the impact of Mo on ductility response is relatively small.

Table 2 – Mechanical properties determined by tensile testing in air and hydrogen atmosphere. Alloy 11 serves as reference for elements Si, S and Mn while alloy 11-R does it for Mo and Cr elements.

Element	Material	R_p [MPa]		R_m [MPa]		A [%]		Z [%]		RZ [%]
		H_2	air	H_2	air	H_2	air	H_2	air	H_2/air
Mo	11-Mo	223	232	641	647	64	67	50	81	62
	11-R	214	220	623	641	67	73	43	81	53
Ni	2	184	185	581	598	73	82	45	81	55
	3	191	195	596	648	61	77	39	81	48
Si	11	190	211	605	655	58	75	40	81	49
	9	223	224	615	700	49	75	33	82	40
S	1	214	222	633	681	59	72	39	68	57
Cr	11-Cr	213	225	631	640	69	68	62	82	76
Mn	8	216	216	587	737	34	64	21	81	26
Ref.	12	222	229	597	586	71	68	81	81	99
	CN0.96	549	563	805	1025	21	67	13	63	21

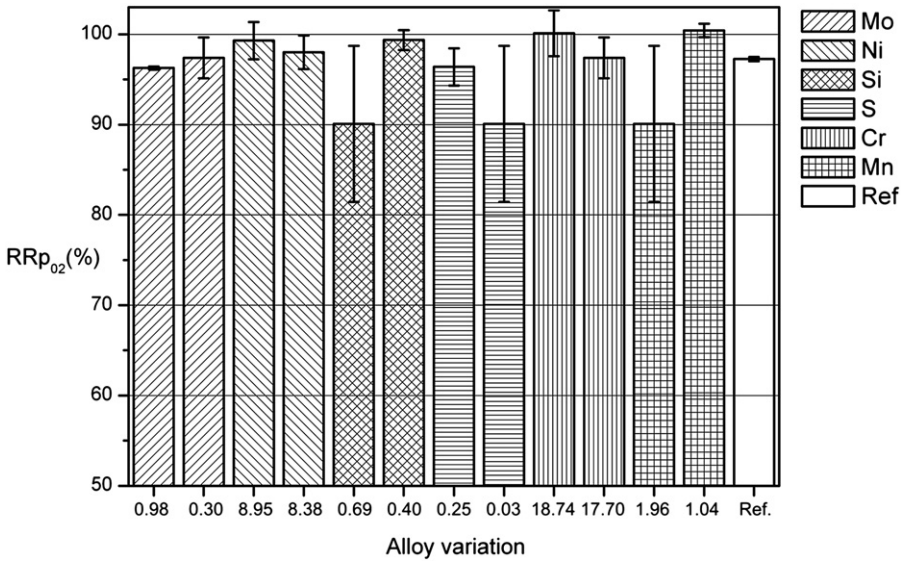

Fig. 3 – Relative yield strength results $\left(\mathbf{RRp_{O_2}} = \frac{\mathbf{Rp_{H_2}}}{\mathbf{Rp_{air}}} \times \mathbf{100}\right)$.

3.2. *Ferrite equivalent and* Md_{30}

Fig. 7 relates the ferrite equivalent value for the hydrogen tested specimens to their corresponding reduction of area. Taking into account the ferrite equivalent value before testing ($F.E._0$) in Table 4, it is clear that the change in the affected volume is due to the formation of strain-induced martensite during plastic deformation. In consequence, a higher tendency to martensite formation is coincident with a more brittle failure, in agreement with other investigations [16–18]. This experimental result is similarly represented by the M_{d30} empirical formula (cf. Eq. (1)) and depicted in Fig. 8. This parameter indicates the temperature at which a true strain of 30% is sufficient for transforming 50% of the austenite into martensite. Therefore, decreasing temperatures are related to a higher stability of the parent phase which turns into a higher ductility in the presence of external hydrogen.

3.3. *Austenite stability by means of thermodynamic calculations*

Difference between austenite and ferrite Gibbs free energy were calculated according to Eq. (2) and employed as an approximation to the martensitic transformation driving force. Corresponding results are shown in Table 4. As can be seen, negative values denote that the bcc phase is thermodynamically stable at room temperature for the investigated compositional range. In the same manner as done for ferrite equivalent and M_{d30}, Fig. 9 shows the reduction of area in hydrogen atmosphere as a function of chemical free energy change. Here, a higher $\Delta G_{\gamma/\alpha}$ represents a lower chemical driving force available for the martensitic transformation [19]. Therefore, at the same testing conditions, as long as the chemical driving force decreases, a higher mechanical driving force is required for promoting the martensitic

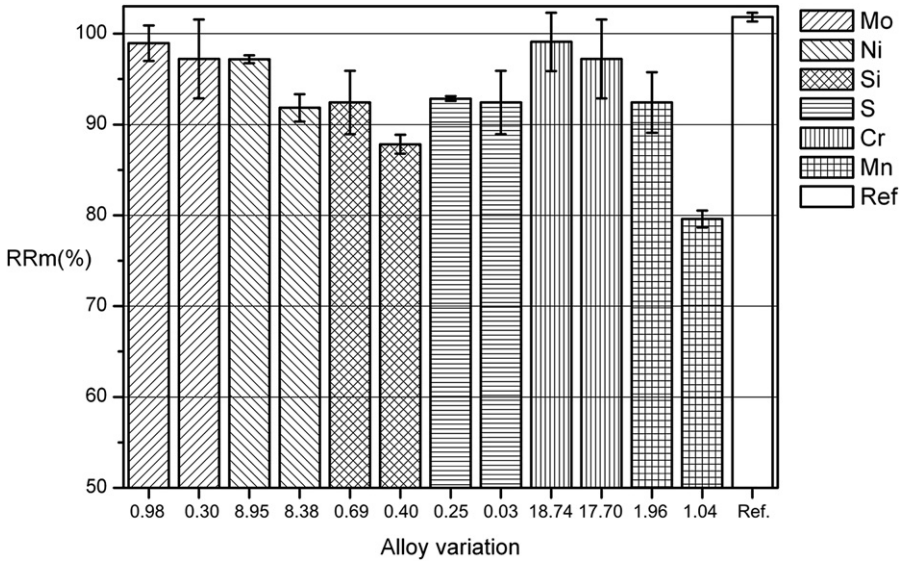

Fig. 4 – Relative tensile strength results $\left(\mathbf{RRm} = \frac{\mathbf{Rm_{H_2}}}{\mathbf{Rm_{air}}} \times \mathbf{100}\right)$.

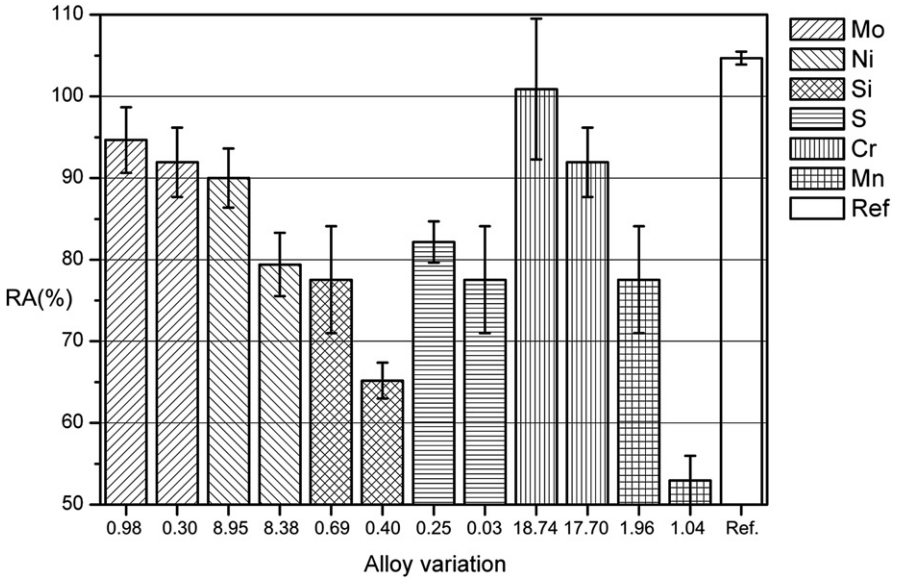

Fig. 5 – Relative elongation to rupture results ($RA = \frac{A_{H_2}}{A_{air}} \times 100$).

transformation, which means that the fcc phase become more stable. This situation is more clearly visualized in Fig. 10, where ferrite equivalent values increase with chemical driving force for three different materials with similar uniform elongation. Once again, a higher stability of the parent phase is associated with an improved ductility response.

4. Discussion

4.1. *Mechanical properties*

Tensile testing is commonly used for studying the influence of hydrogen on material's mechanical properties. In the case of austenitic stainless steel, some differences are encountered between a hydrogen gas environment and a hydrogen precharged condition. For hydrogen precharged conditions, yield strength increases with hydrogen content for both foils and bulk specimens. This behaviour is interpreted in terms of a solid solution strengthening effect [20,21], or as a consequence of hydrogen induced strain localization [22]. In contrary, the same property is not significantly affected during testing in hydrogen gas environment [23–25], as also found in the present work (c.f. Fig. 3). No change in yield strength during hydrogen gas environment testing may indicate that hydrogen is not able to penetrate into the fcc lattice as a consequence of its low diffusivity and a comparatively short timescale for testing. As a consequence, no change in yield strength can be expected if no hydrogen is dissolved into the metal matrix.

In a similar way, an increase of tensile strength is generally observed for precharged specimens [20] while testing in gas environment can lead to diverse results. In particular, San

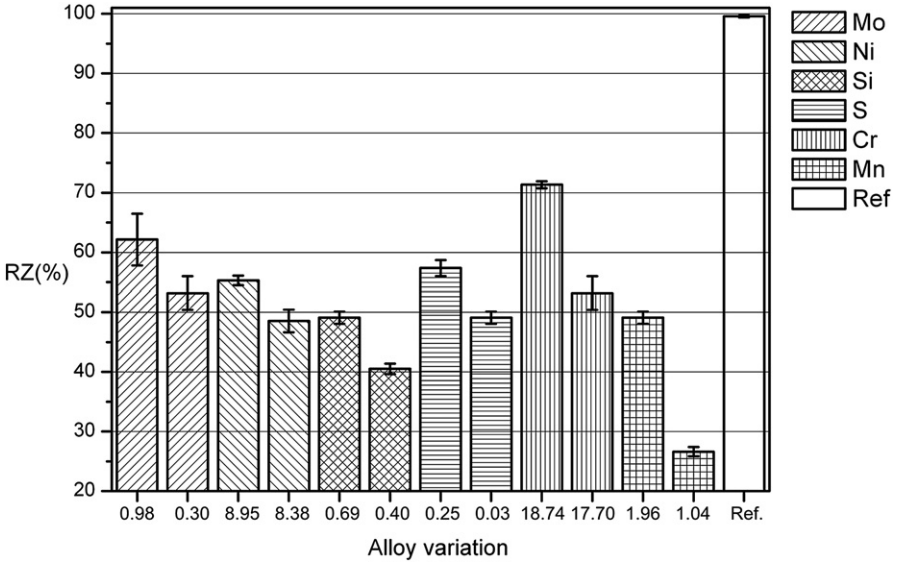

Fig. 6 – Relative reduction of area results ($RZ = \frac{Z_{H_2}}{Z_{air}} \times 100$).

Table 3 – Alloying element impact on ductility response.

Element	$Element_{ratio}$	A_{ratio}	Z_{ratio}	A_r Norm.	Z_r Norm.	Impact factor
Mo	3.32	0.94	1.16	0.28	0.35	0.10
Ni	1.06	1.20	1.13	1.13	1.06	1.20
Si	1.70	1.18	1.20	0.69	0.70	0.49
Cr	1.05	1.01	1.45	0.96	1.37	1.32
Mn	1.88	1.71	1.85	0.90	0.98	0.89

Marchi et al. [23] reported a reduction in tensile strength for cases where a relative reduction of area (RZ) lower than 50% is verified. This condition is also seen in the current results. As shown in Fig. 4, higher reductions in tensile strength take place for alloys 9 ($Si_{0.4}$) and 8 ($Mn_{1.04}$) which feature a RZ $\leq$ 50%, whereas the rest of alloys remain in the 90–100% RRm band.

While yield and tensile strength are not seriously affected under current testing conditions, the material's ductility response is clearly weakened. Relative elongation to rupture (RA) in Fig. 5 shows a higher ductility for alloy 2 ($Ni_{8.95}$) but also and more interesting, a quite positive influence of Si, Cr and Mn addition in alloys 11($Si_{0.68}$), 11-Cr ($Cr_{18.74}$) and 11 ($Mn_{1.96}$), respectively. In the same figure, it is possible to identify a trend which indicates that a higher content on the selected element addition leads to higher elongation to rupture. Relative reduction of area resulted in the most sensitive property to hydrogen environmental embrittlement phenomena. Similarly to the elongation to rupture results, the higher alloyed material revealed an improvement of ductility with an outstanding response for the 11-Cr ($Cr_{18.74}$) alloy, c.f. Fig. 6.

4.2. *Effects of alloying elements*

Elongation to rupture and reduction of area results have shown that a higher alloying degree leads to a better ductility response for all investigated elements. In a first view, this result can be globally understood as the decrease in M_{d30} temperature with an increasing alloying content, as depicted in Eq. (1) and Fig. 8. Nevertheless, the effect of every alloying element can be individually discussed if some key aspects concerning hydrogen embrittlement are considered. Regarding current knowledge, the macroscopic brittle behavior can be related to a highly ductile mechanisms on the microscopic scale. This theory, known as HELP (hydrogen enhanced localized plasticity), was developed by Birnbaum et al. [7] based on a continuum mechanical approach and shows that dislocations mobility is increased and pile-up distance reduced by the presence of solute hydrogen atoms. Consistent with the previous interpretation, another approach has been achieved by considering the change caused by hydrogen in electronic structure of metallic materials [26–28]. In this case, ab initio calculations and experimental results indicate that hydrogen enhances the metallic character of interatomic bonding by increasing the density of states (DOS) at the Fermi level which results in a decrease of the shear modulus and therefore in plastic strain localization. Keeping in mind both theories, the role of alloying elements is discussed in relation to their influence on microstructural aspects capable of hindering hydrogen and dislocation mobility, together with their capability to counteract hydrogen influence on the material's electronic structure.

Table 4 – Ferrite equivalent before and after tensile testing, M_{d30} and $\Delta G_{\gamma/\alpha}$ of the investigated austenitic stainless steel.

Element	Material	F.E.$_0$ [vol%]	F.E.$_f$ [vol%]	M_{d30} [C]	$\Delta G_{\gamma/\alpha}$ [J/mol]
Mo	11-Mo	1.40	5.3	−41	−2429
	11-R	0.40	8.1	−30	−2443
Ni	2	0.13	8.6	−28	−2476
	3	0.16	10	−16	−2519
Si	11	0.30	10.2	−23	−2477
	9	0.40	11.7	−13	−2493
S	1	0.11	6.1	−22	−2540
Cr	11-Cr	1.76	5.6	−42	−2420
Mn	8	0.13	14	−1.6	−2679
Ref.	12	0.15	0.24	−143	−2128
	CN0.96	0	0	−292	1186

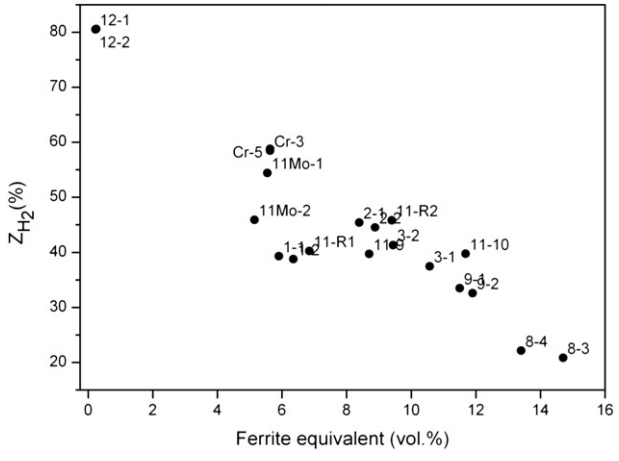

Fig. 7 – Reduction of area for hydrogen tested specimens as a function of ferrite equivalent.

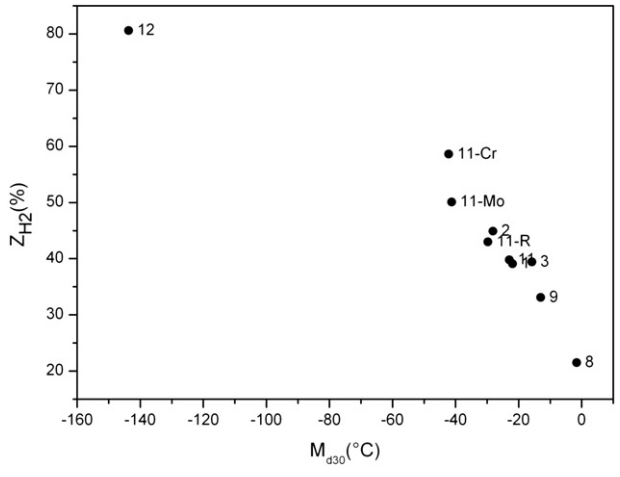

Fig. 8 – Reduction of area in hydrogen atmosphere as a function of M_{d30} temperature.

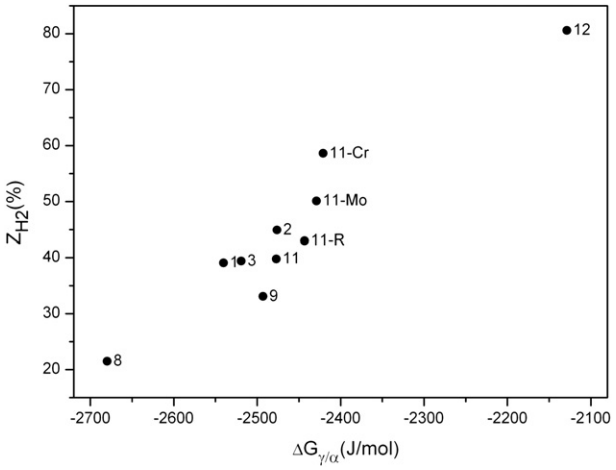

Fig. 9 – Reduction of area in hydrogen atmosphere versus Gibbs free energy difference between fcc and bcc phase.

Increasing sulphur content is expected to promote manganese sulphide precipitation in the investigated steels. Interfaces of such non-metallic inclusions have been identified as trapping sites for hydrogen atoms and being responsible of embrittlement reduction in resulfurized steels [29,30]. However, the same effect is not observed at current testing conditions. As can be seen in Table 2, values for elongation to rupture and reduction of area in hydrogen are very similar for both high and low sulphur content. Therefore, the apparent improvement of relative reduction of area observed in Fig. 6 is attributed to a poorer performance in air testing resulting from a higher MnS density.

In the case of *Mo*, ductility improvement can be mainly correlated to its contribution to M_{d30} temperature. However, its relatively low impact in combination with its cost driving character turn it as an unattractive alloying alternative.

Si alloying shows to increase resistance to hydrogen embrittlement of precharged austenitic steels specimens [31].

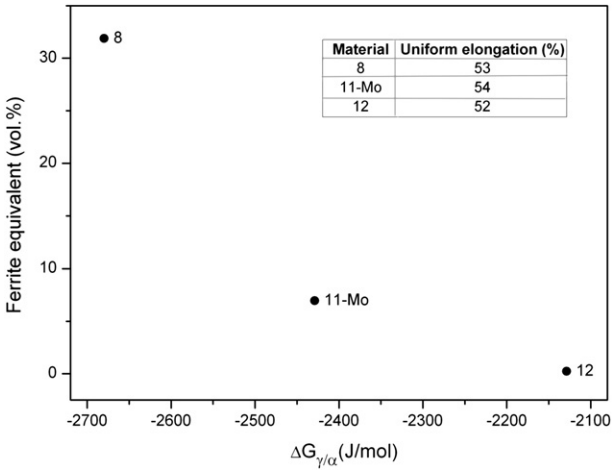

Fig. 10 – Ferrite equivalent as function of Gibbs free energy difference at similar uniform elongation (air tested specimens).

Moreover, an addition of 1.5 wt.% Si in Fe-Mn steels has shown to be able to hinder the movement of Shockley partial dislocations by introducing vacancy defects and a high lattice distortion [32]. Consequently, a positive influence of Si is expected. In particular, an upper limit of 2 wt.% may be suggested due to once this value is overcome, stacking fault energy (SFE) is strongly decreased. The last can lead to two detrimental features like strain-induced martensite formation and the occurrence of slip-planarity [33].

Alloying with *Mn* seems to be capable of contributing to hydrogen embrittlement reduction in different manners. Beyond stabilizing the fcc phase, it increases SFE in Fe-Mn and Fe–Cr–Ni alloys [34,35] and decreases the concentration of free-electrons in Cr-Ni steels [28,36]. All these effects, together with its low cost and availability constitute Mn as a serious candidate for further developments of new alloys with reduced embrittlement suceptibility. Nevertheless, in the particular compositional range investigated in this work, the main Mn-contribution might be related to its fcc-stabilizing effect.

Austenitic stainless steels show an increased resistance to hydrogen-assisted fracture with higher *Ni* contents. This effect has been related to Ni influence on increasing austenite stability and stacking fault energy. While a more stable austenitic phase is less susceptible to the $\gamma \rightarrow \alpha'$ phase transformation [3,37], a higher stacking fault energy results in a more homogeneous deformation by reducing slip planarity [38]. In this context, several investigations suggest a Ni content superior to 12 wt.% for providing embrittlement resistance even at low temperatures [25,38]. As shown by current results, the last criterion is also verified by the reference material (12). However, similarly to Mo, cost efficiency requirements make a reduction of Ni contents mandatory for further alloy developments.

Beyond its outstanding contribution within the investigated compositional range, the role of *Cr* cannot be straightforwardly elucidated beyond its input to M_{d30} temperature. Alloying with Cr may affect both the crystal and electron structure of the material and generate a competition among different mechanisms which could define the overall contribution of the Cr alloying process. Concerning microstructural aspects, Cr addition can decrease the SFE of austenitic stainless steels [39,40] and promote short-range ordering in the Ni–Cr–Fe system [41]. Both aspects enhance slip planarity and in consequence could be related to a higher hydrogen embrittlement susceptibility. In particular, in the Ni–Cr–Fe system, Symons et.al. found an extreme ductility loss coincident with a minimum in SFE for Cr contents higher than 25 wt.% but a positive contribution for contents lower than 15 wt.% [41]. Regarding the Cr effect on electron structure, Beskrovni et al. [42] and Gavriljuk et al. [43] have shown that a reduction in free electrons concentration occurs by alloying with Cr in Fe-Cr-Ni-N and iron-based austenitic alloys, respectively. This effect is exactly the opposite to what hydrogen causes on electron structure for the same systems [27]. Therefore, the beneficial effect of Cr alloying might be related to its counteracting role in the material's electronic structure. Finally, considering both crystal and electron structure contribution together with the current work and findings of Symons et al., it might be possible that for a Cr

content higher than 20 wt.% microstructural aspects prevail over the electronic ones leading to a decrease in hydrogen embrittlement resistance for austenitic steels.

4.3. *Thermodynamic calculations*

The evaluation of austenite stability as the difference in chemical free energy between the fcc and bcc phase indicates that the material's susceptibility to hydrogen embrittlement decreases by lowering the available driving force for the corresponding phase transformation (c.f. Fig. 9). The last is in agreement with experimental results which show higher ductility response by decreasing the material's volume affected by the strain-induced martensite formation (c.f. Fig. 7). In this context, a major interest arose regarding the evaluation of a fully stable austenitic steel against hydrogen embrittlement. The selected alloy was a high-C high-N austenitic steel designated as CN0.96, with the chemical composition presented in Table 1. In the same manner as carried out for the rest of alloys, change in chemical free energy was calculated according to Eq. (2). In opposition to previous cases, the difference in Gibbs free energy resulted in a positive value; indicating that the fcc phase is thermodynamically stable at room temperature for this alloy (c.f. Table 4). This thermodynamic assessment was consistent with ferrite equivalent measurements which shows no magnetic phases neither before nor after air and hydrogen gas testing. Mechanical properties were evaluated in the same conditions as described in paragraph 2.2, and corresponding results are presented in Table 2. Here, a 13% of reduction of area in hydrogen gas atmosphere clearly shows a severe embrittlement effect for this material. Taking into account that strain-induced martensite formation is completely avoided during tensile testing, localized deformation resulting from a compositional effect might be governing the hydrogen-assisted fracture [44]. For the case of metastable austenitic stainless steel, hydrogen-assisted fracture has been generally related to strain-induced martensite formation [18,37,45,46]. In addition, an alternative explanation has been proposed by San Marchi *et.al.*, relating chemical composition and environmental conditions (*e.g.* temperature) to localization of deformation [47]. In this regard, the authors consider that both compositional and microstructural effects have to be incorporated in new alloys designing. In particular, stable austenitic structures would be desirable to avoid martensite formation and simultaneously promote a uniform deformation by featuring relatively high stacking fault energy. Having in mind these two approaches to hydrogen-assisted fracture of metastable austenitic stainless steels, the alloy design process could be primarily based on thermodynamic calculations pointing to chemical compositions capable of achieving certain austenite stability. In particularly, a $\Delta G_{\gamma/\alpha}$ value of −2100 [J/mol] might be used as a starting point. Since it corresponds to the reference material employed in this study and is additionally reported as a threshold magnitude for the $\gamma \rightarrow \alpha'$ phase transformation [48]. Once more, as shown by the CN0.96 results, it must be kept in mind that a fully stable austenitic structure might be necessary but not sufficient to assure a complete resistant against HEE.

5. Summary

In this work, the influence of the alloying elements Mo, Ni, Si, S, Cr and Mn on the susceptibility of austenitic stainless steels to hydrogen environment embrittlement was evaluated by modifying an AISI type 304 base chemical composition. Concerning mechanical properties, yield and tensile strength were slightly affected by the external hydrogen pressure. On the other hand, reduction of area appears as the most sensitive parameter to present testing conditions. In particular, relative reduction of area results indicate, with the exception of Ni, an outstanding contribution to ductility improvement by Si, Mn and Cr addition over the others alloying elements. These results were consistent with steel's proneness to strain-induced martensite formation, both experimentally and thermodynamically verified. Concerning further alloy developments, Si and Cr additions are expected to have a positive effect for contents lower than 2 and 20 wt%, respectively; whereas Mn addition would be only restricted by technological limitations. In this scope, an austenite phase stability characterized by a difference of −2100 [J/mol] between fcc and bcc Gibbs free energy is recommended. Although it might not be sufficient to assure a complete resistance to hydrogen environment embrittlement.

Acknowledgment

The authors gratefully acknowledge the financial support of the Bundesministerium für Wirtschaft und Technologie (BMWi (gs1)) under contract number 0327802D. Tensile tests in hydrogen were performed at "The Welding Institute" (TWI, Cambridge, UK).

REFERENCES

[1] Birnbaum HK. Hydrogen embrittlement. Encyclopedia of Materials: Science and Technology; 2001:3887–9.
[2] Eliezer D, Chakrapani DG, Altstetter CJ, Pugh EN. Influence of austenite stability on the hydrogen embrittlement and stress–corrosion cracking of stainless–steel. Metallurgical Transactions A–Physical Metallurgy and Materials Science 1979;10(7):935–41.
[3] Han G, He J, Fukuyama S. Effect of strain–induced martensite on hydrogen environment embrittlement of sensitized austenitic stainless steels at low temperatures. Acta Materialia 1998;46(13):4559–70.
[4] Briant CL. Hydrogen assisted cracking of type–304 stainless–steel. Metallurgical Transactions A–Physical Metallurgy and Materials Science 1979;10(2):181–9.
[5] Toribio J. Effects of strain rate and notch geometry on hydrogen embrittlement of AISI type–316l austenitic stainless–steel. Fusion Engineering and Design 1991;16: 377–86.
[6] C.Izawa, S.Wagner, M.Martin, S.Weber, A.Bourgeon, R. Pargeter, et al, SIMS study on the surface chemistry of stainless steel AISI 304 cylindrical tensile test samples showing hydrogen embrittlement: International Symposium on Metal–Hydrogen–Systems, 2010, Moscow, Journal of

Alloys and Compounds, MH2010 Symposium Proceedings, 2011, doi:10.1016/j.jallcom.2010.12.143.
[7] Birnbaum HK, Sofronis P. Hydrogen–enhanced localized plasticity – a mechanism for hydrogen–related fracture. Materials Science and Engineering A–Structural Materials Properties Microstructure and Processing 1994;176(1–2): 191–202.
[8] Louthan M, Caskey GR, Donovan JA, Rawl DE. Hydrogen embrittlement of metals. Materials Science and Engineering 1972;10(6):357–68.
[9] Nohara K, Ono Y, Ohashi N. Composition and grain size dependencies of strain–induced martensitic transformation in metastable austenitic stainless steels. ISIJ International 1977;63(5):212–22.
[10] Haidemenopoulos GN, Grujicic M, Olson GB, Cohen M. Thermodynamics–based alloy design criteria for austenite stabilization and transformation toughening in the Fe–Ni–Co system. Journal Of Alloys And Compounds 1995; 220(1–2):142–7.
[11] Ishida K. Direct estimation of stacking fault energy by thermodynamic analysis. Physica Status Solidi A 1976;36: 717–28.
[12] Miodownik P. Calculation of stacking–fault energies in Fe–Ni–Cr alloys. CALPHAD–Computer Coupling of Phase Diagrams and Thermochemistry 1978;2(3):207–26.
[13] Saunders N, Miodownik AP. CALPHAD–Calculation of phase diagrams. In: A comprehensive guide, vol. 1. Oxford: Pergamon Materials Series, Pergamon; 1998.
[14] Lukas SFHL, Sundman B. Computational thermodynamics: the calphad method. Cambridge Universiity Press; 2007. Vol.
[15] Spencer J. A brief history of calphad. CALPHAD–Computer Coupling of Phase Diagrams and Thermochemistry 2008; 32(1):1–8.
[16] Perng TP, Altstetter CJ. Comparison of hydrogen gas embrittlement of austenitic and ferritic stainless–steels. Metallurgical and Materials Transactions A–Physical Metallurgy and Materials Science 1987;18(1):123–34.
[17] Perng TP, Altstetter CJ. Hydrogen effects in austenitic stainless–steels. Materials Science and Engineering A 1990; 129(1):99–107.
[18] Kanezaki T, Narazaki C, Mine Y, Matsuoka S, Murakami Y. Effects of hydrogen on fatigue crack growth behavior of austenitic stainless steels. International Journal of Hydrogen Energy 2008;33(10):2604–19.
[19] .Olson GB, Owen WS. Martensite. ASM International; 1992.
[20] Abraham DP, Altstetter CJ. The effect of hydrogen on the yield and flow–stress of an austenitic stainless–steel. Metallurgical and Materials Transactions A–Physical Metallurgy and Materials Science 1995;26(11):2849–58.
[21] Long QY, Fan CG, Xing ZS, Li YY. The effects of h on the mechanical–behavior of austenitic stainless–steels at room–temperature. Metallurgical and Materials Transactions A–Physical Metallurgy and Materials Science 1994;25(5):1015–23.
[22] Birnbaum H. Hydrogen effects on deformation – relation between dislocation behaviour and the macroscopic stress–strain behaviour. Scripta Metallurgica et Materialia 1994;31:149–53.
[23] San Marchi C, Michler T, Nibur KA, . Somerday BP. On the physical differences between tensile testing of type 304 and 316 austenitic stainless steels with internal hydrogen and in external hydrogen. International Journal of Hydrogen Energy 2010;35(18):9736–45.
[24] Michler T, Yukhimchuk AA, Naumann J. Hydrogen environment embrittlement testing at low temperatures and high pressures. Corrosion Science 2008;50(12):3519–26.
[25] Michler T, Naumann J. Hydrogen environment embrittlement of austenitic stainless steels at low temperatures. International Journal of Hydrogen Energy 2008;33(8):2111–22.
[26] Gavriljuk VG, Shivanyuk VN, Shanina BD. Change in the electron structure caused by C, N and H atoms in iron and its effect on their interaction with dislocations. Acta Materialia 2005;53(19):5017–24.
[27] Gavriljuk VG, Shyvanyuk VN, Teus SM. Hydrogen brittleness of austenitic steels. Materials Science Forum (638–642):104–9. doi:10.4028, www.scientific.net/MSF.638-642.104; 2010.
[28] V.G. Gavriljuk, B.D. Shanina, V.N. Shyvanyuk, S.M. Teus, Electronic effect on hydrogen brittleness of austenitic steels, Journal of Applied Physics 108. URL doi:10.1063/1.3499610.
[29] LUU WC, WU JK. Effects of sulfide inclusion on hydrogen transport in steels. Materials Letters 1995;24(1–3):175–9.
[30] Kobayashi Y, Szklarskasmialowska Z. A study of the hydrogen–induced degradation of 2 steels differing in sulfur–content. Metallurgical Transactions A–Physical Metallurgy and Materials Science 1986;17(12):2255–63.
[31] Shivanyuk VN, Foct J, Gavriljuk VG. On a role of hydrogen–induced epsilon–martensite in embrittlement of stable austenitic steel. Scripta Materialia 2003;49(6):601–6.
[32] Huang SK, Li N, Wen Y, Teng J, Ding S, Xu Y. Effect of si and cr on stacking fault probability and damping capacity of fe–mn alloy. Materials Science and Engineering A–Structural Materials Properties Microstructure and Processing 2008; 479(1–2):223–8.
[33] Takemoto T, Murata Y, Tanaka T. Effects of alloying elements and thermomechanical treatments on mechanical and magnetic–properties of cr–ni austenitic stainless–steel. ISIJ International 1990;30(8):608–14.
[34] Li JC, Zhao M, Jiang Q. Alloy design of femnsicrni shape–memory alloys related to stacking–fault energy. Metallurgical and Materials Transactions A–Physical Metallurgy and Materials Science 2000;31(3):581–4.
[35] Jun JH, Choi CS. Change in stacking–fault energy with mn content and its influence on the damping capacity of the austenitic phase in fe–high mn alloys. Journal of Materials Science 1999;34(14):3421–5.
[36] Petrov YN. On the electron structure of Mn–, Ni– and Cr–Ni–Mn austenite with different stacking fault energy. Scripta Materialia 2005;53(10):1201–6.
[37] Zhang L, Wen M, Imade M e a. Effect of nickel equivalent on hydrogen gas embrittlement of austenitic stainless steels based on type 316 at low temperatures. Acta Materialia 2008; 56(14):3414–21.
[38] Marchi CS, Somerday BP, Tang X, Schiroky GH. Effects of alloy composition and strain hardening on tensile fracture of hydrogen–precharged type 316 stainless steels. International Journal of Hydrogen Energy 2008;33(2):889–904.
[39] Schramm RE, Reed R. Stacking fault energies of seven commercial austenitic stainless steels. Metallurgical and Materials Transactions A 1975;6(8):1345–51. 1975/08/01/.
[40] Vitos L, Nilsson JO, Johansson B. Alloying effects on the stacking fault energy in austenitic stainless steels from first–principles theory. Acta Materialia 2006;54(14):3821–6.
[41] Symons DM. Hydrogen embrittlement of Ni–Cr–Fe alloys. Metallurgical and Materials Transactions A–Physical Metallurgy and Materials Science 1997;28(3):655–63.
[42] Beskrovni A, Danilkin S, Fuess H, Jadrowski E, Neova-Baeva M, Wieder T. Effect of cr content on the crystal structure and lattice dynamics of fccfe–cr–ni–n austenitic alloys. Journal of Alloys and Compounds 1999;291(1–2): 262–8.
[43] Gavriljuk VG, Shanina BD, Berns H. On the correlation between electron structure and short range atomic order in iron–based alloys. Acta Materialia 2000;48:3879–93.
[44] Nibur KA, Somerday BP, Balch DK, San Marchi C. The role of localized deformation in hydrogen–assisted crack

propagation in 21Cr–6Ni–9Mn stainless steel. Acta Materialia 2009;57(13):3795–809.
[45] Mine Y, Narazaki C, Murakami K, Matsuoka S, Murakami Y. Hydrogen transport in solution–treated and pre–strained austenitic stainless steels and its role in hydrogen – enhanced fatigue growth. International Journal of Hydrogen Energy 2009;34:1097–107.
[46] Martin M, Weber S, Izawa C, Pundt A, Wagner S, Theisen W. Influence of machining–induced martensite on hydrogen–assisted fracture of AISI type 304 austenitic stainless steel. International Journal Of Hydrogen Energy 2011;36(17):11195–206.
[47] San Marchi C, Nibur K, Balch D, Somreday B, Tang X, Schiroki H, et al. Effects of hydrogen on materials: Proceedings of the 2008 international hydrogen conference. ASM International; 2009. 88–96.
[48] Borgenstam A, Hillert M. The driving force for lath and plate martensite and the activation energy for isothermal martensite in ferrous alloys. Journal de Physique 1997;IV: 23–8.